MNRAS **000**, 1–9 (2016) Preprint 25 January 2016 Compiled using MNRAS LATEX style file v3.0

Limits on the significant mass-loss scenario based on the globular clusters of the Fornax dwarf spheroidal galaxy

P. Khalaj⋆ and H. Baumgardt†
School of Mathematics and Physics, University of Queensland, St. Lucia, QLD 4072, Australia

arXiv:1512.05260v2 [astro-ph.GA] 21 Jan 2016

Accepted 2015 December 14. Received YYY; in original form ZZZ

ABSTRACT

Many of the scenarios proposed to explain the origin of chemically peculiar stars in globular clusters (GCs) require significant mass-loss ($\geq 95\%$) to explain the observed fraction of such stars. In the GCs of the Fornax dwarf galaxy significant mass-loss could be a problem. Larsen et al. (2012) showed that there is a large ratio of GCs to metal-poor field stars in Fornax and about $20-25\%$ of all the stars with [Fe/H] < -2 belong to the four metal-poor GCs. This imposes an upper limit of $\sim 80\%$ mass-loss that could have happened in Fornax GCs. In this paper, we propose a solution to this problem by suggesting that stars can leave the Fornax galaxy. We use a series of N-body simulations, to determine the limit of mass-loss from Fornax as a function of the initial orbital radii of GCs and the speed with which stars leave Fornax GCs. We consider a set of cored and cuspy density profiles for Fornax. Our results show that with a cuspy model for Fornax, the fraction of stars which leave the galaxy, can be as high as $\sim 90\%$, when the initial orbital radii of GCs are $R = 2-3$ kpc and the initial speed of stars is $v > 20\,\mathrm{km\,s^{-1}}$. We show that such large velocities can be achieved by gas expulsion induced mass-loss but not stellar evolution induced mass-loss. Our results imply that one cannot interpret the metallicity distribution of Fornax field stars as evidence against significant mass-loss in Fornax GCs, if mass-loss is due to gas expulsion.

Key words: methods: numerical – stars: chemically peculiar – stars: formation – globular clusters: general – galaxies: evolution – galaxies: individual: Fornax dSph

1 INTRODUCTION

Almost all GCs in the Milky Way and other galaxies such as the Fornax dwarf spheroidal galaxy (dSph) show light element abundance anomalies and splits in their colour-magnitude diagram which can be attributed to the existence of more than one stellar population in these GCs. Examples of such GCs include ω Cen (Rey et al. 2004), NGC2808 (Piotto et al. 2007; Milone et al. 2015), GCs in Fornax (D'Antona et al. 2013) and M80 (Carretta et al. 2015).

There are several scenarios which have been proposed to explain the origin of chemically peculiar stars in GCs, e.g. fast-rotating massive stars (FRMS; $20-120\,\mathrm{M}_\odot$; Prantzos & Charbonnel 2006; Decressin et al. 2007a,b; Krause et al. 2013, asymptotic giant branch stars (AGB; $4-9\,\mathrm{M}_\odot$; Ventura et al. 2001; D'Ercole et al. 2008), intermediate-mass and massive binaries ($4-100\,\mathrm{M}_\odot$; de Mink et al. 2009) and early disc accretion in low-mass pre-main-sequence stars (polluter mass $M > 10\,\mathrm{M}_\odot$; Bastian et al. 2013). Among these scenarios, FRMS and the AGB scenario are challenged by the so-called mass-budget problem. According to these scenarios, the ejecta of primordial stars which later form chemically peculiar stars make up between 4 and 9 per cent of the initial stellar mass (de Mink et al. 2009), assuming a standard Kroupa (2001) mass function for primordial stars. Unless the initial mass-function of primordial stars was top-heavy, this is not sufficient for the formation of a large fraction of chemically peculiar stars in GCs, which is found to be ~ 70 per cent (Carretta et al. 2010). One possible solution for this problem is that the cluster loses a significant fraction of its primordial stars, i.e. ≥ 95 per cent, to increase the relative fraction of chemically peculiar stars. Two of the mechanisms which can cause a significant mass-loss in GCs are stellar evolution induced mass-loss (D'Ercole et al. 2008; hereafter DE08) and primordial gas expulsion (Khalaj & Baumgardt 2015; hereafter KB15).

It is worthwhile to mention that, the two other mechanisms proposed to explain the origin of abundance anomalies, i.e. binaries (de Mink et al. 2009) and pollution of

⋆ E-mail: pouria.khalaj@uqconnect.edu.au
† E-mail: h.baumgardt@uq.edu

© 2016 The Authors

pre-main sequence low-mass stars by the ejecta of rapidly evolving primordial stars (Bastian et al. 2013) do not suffer from the mass-budget problem if one assumes a close to 100 per cent binary fraction or a large survival time-scale for pre-main sequence disc of chemically peculiar stars. However, Bastian et al. (2015) showed all the proposed models overproduce He for a given change in Na and O. Hence none of the scenarios which has been put forth so far is able to explain all the observed GCs.

Bastian & Lardo (2015) examined an ensemble of 33 Galactic GCs for any correlations between the fraction of chemically peculiar stars and other cluster properties such as the cluster mass and compared them with predictions given in other studies. They argued against the self-enrichment scenario via nucleosynthesis for the Galactic GCs.

Larsen et al. (2012) and Larsen et al. (2014) found a large ratio of GCs to metal poor field stars in dwarf galaxies. Since any mass-loss from GCs will contribute to the overall metallicity distribution of field stars, this discovery imposes an upper limit for the maximum mass that can be lost by a GC in Fornax. This upper limit which is about 4−5 times the current cluster mass (Larsen et al. 2012; de Boer & Fraser 2015) is below the required limit of the significant mass-loss scenario ($\geq$ 95 per cent). In addition, Fornax GCs are very similar to Galactic GCs in terms of abundance anomalies, mass and luminosities (D'Antona et al. 2013; Larsen et al. 2012; de Boer & Fraser 2015). This raises the question if significant mass-loss could have happened in Fornax GCs or not.

If the speeds by which the unbound stars leave the GC is large enough then these stars can be stripped off by the Milky Way and leave the gravitational field of Fornax, hence do not contribute to the metallicity distribution of field stars. In this case the upper limit of 4-5 times more massive from Larsen et al. (2012) does not apply any more.

In this paper we aim to answer this question by doing N-body simulations of stars which initially belong to GCs and then become unbound (hereafter runaway stars). We follow their trajectory over a Hubble time to see whether they leave the Fornax dSph or not. The current paper is structured as follows: In the next section we explain the setup and the details of our N-body simulations. In Section 3 we bring the results of the simulations. In Section 4 we discuss the implications of our results for the formation scenarios of chemically peculiar stars in dwarf galaxies and conclude our work in Section 5.

2 N-BODY SIMULATIONS

2.1 Milky Way and Fornax Models

We use a logarithmic potential field to model the Milky Way halo

$$\Phi(R) = \frac{1}{2}V_\infty^2 \ln\left(R_c^2 + R^2\right) \quad (1)$$

where R_c is the core-radius and V_∞ is the asymptotic velocity. We assume $R_c = R_\odot = 8300\,\mathrm{pc}$ and $V_\infty = V(R_\odot) = 239\,\mathrm{km\,s^{-1}}$ (McMillan 2011; Irrgang et al. 2013). In a right-handed Galactocentric coordinate system whose $x-$, $y-$ and z axes point towards the Sun, the direction of the orbital motion of the Sun and the North Galactic pole respectively, the current position and velocity vectors of Fornax are $\vec{R} = (-41.3\,\mathrm{kpc}, -51.0\,\mathrm{kpc}, -134.1\,\mathrm{kpc})$ and $\vec{V} = (-38\,\mathrm{km\,s^{-1}}, -158\,\mathrm{km\,s^{-1}}, 114\,\mathrm{km\,s^{-1}})$ respectively (Pawlowski & Kroupa 2013). By numerical integration of the Fornax orbit in the Milky Way potential field, given by equation (1), we find that the current distance, perigalactic distance, apogalactic distance, eccentricity, orbital inclination and radial and azimuthal periods of Fornax are $R = 149.3\,\mathrm{kpc}$, $R_\mathrm{p} = 99.4\,\mathrm{kpc}$, $R_\mathrm{a} = 154.7\,\mathrm{kpc}$, $e \equiv (R_\mathrm{a} - R_\mathrm{p})/(R_\mathrm{a} + R_\mathrm{p}) = 0.22$, $i = 81^\circ$, $T_r = 2.4\,\mathrm{Gyr}$ and $T_\psi = 3.3\,\mathrm{Gyr}$.

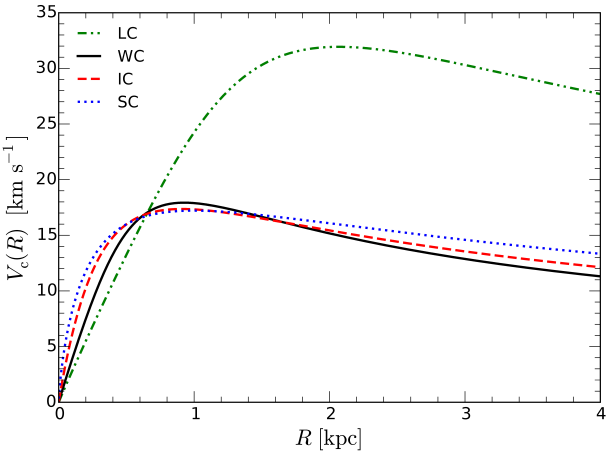

Figure 1. The Fornax velocity curves as a function of radius according to different models given by equation (2). Compared to cuspy models, the large core model predicts a larger circular velocity for $R > 0.8\,\mathrm{kpc}$ due to its larger enclosed mass.

For the density profile of Fornax, we use the recent models of Cole et al. (2012) which are derived by applying Markov Chain Monte Carlo (MCMC) analysis to the kinematic data of more than 2000 stars in Fornax. These models have the benefit of including both the stellar and dark matter content of Fornax and that they cover a wide-range of inner density slopes (Cole et al. 2012). The models are designated by large core (LC), weak cusp (WC), intermediate cusp (IC) and steep cusp (SC), all of which have the following form for the density profile

$$\rho(r) \propto \left(\frac{r}{r_\mathrm{s}}\right)^{-\gamma_0} \left(1 + \left(\frac{r}{r_\mathrm{s}}\right)^{\eta}\right)^{\frac{\gamma_0 - \gamma_\infty}{\eta}} \mathrm{sech}(r/10\,\mathrm{kpc}) \quad (2)$$

where r_s is a scale radius, $\gamma \equiv -\mathrm{d}\ln\rho/\mathrm{d}r$ is the logarithmic density slope and η is a constant. The best-fitting parameters are found using MCMC. Table 1 summarizes the characteristics of these models.

The models describe the observed velocity dispersion profile of Fornax very well, however they do not lead to analytical relations for other dynamical parameters such as the enclosed mass at each radius $M(R)$. As a result we used numerical integration to find $M(R)$ (needed for force calculations) and the circular orbital velocity $V_\mathrm{c}(R)$ (needed for initial conditions) and verified our results by comparing with Fig. 2 of Cole et al. (2012). Figure 1 illustrates $V_\mathrm{c}(R)$ for different models adopted in this study. The effect that the choice of the density profile of Fornax has on our results is discussed in Section 3.

Table 1. Adopted models in this study for the density profile of the Fornax dSph given by equation (2). γ_0, γ_∞, η, r_s and the total mass are directly taken from Table 2 of Cole et al. (2012). V_c is the circular velocity derived by numerical integration (Fig. 1) and tidal radii are derived from equation (3).

Model	Total Mass	γ_0	γ_∞	η	r_s	Tidal Radius	V_c (500 pc)	V_c (1000 pc)	V_c (3000 pc)
-	$10^8\,M_\odot$	-	-	-	kpc	kpc	km s^{-1}	km s^{-1}	km s^{-1}
LC	8.00	0.07	4.65	3.70	1.40	6.7	13.3	24.2	30.3
WC	1.23	0.08	4.65	2.77	0.62	3.6	15.2	17.9	12.8
IC	1.51	0.13	4.24	1.37	0.55	3.8	16.0	17.3	13.6
SC	1.98	0.52	4.27	0.93	0.80	4.2	16.0	17.2	14.6

2.2 Tidal Radius of Fornax and Escape Criterion

For each of the density profiles introduced in Section 2.1, we calculate the tidal radius R_t of Fornax. The tidal radii are needed later as they specify the ejection criteria from Fornax.

The tidal radius of a stellar system with mass M, on a circular orbit with radius R_G around a host galaxy with a logarithmic potential specified by equation (1), is

$$R_t = \left(\frac{GM}{2V_\infty^2}\right)^{\frac{1}{3}} R_G^{\frac{2}{3}} \left(\left(\frac{R_c}{R_G}\right)^2 + 1\right)^{\frac{2}{3}} \quad (3)$$

The derivation details of this equation are given in Appendix A.

Baumgardt & Makino (2003) and Webb et al. (2013, 2014) showed that stellar systems with eccentric orbits around a host galaxy have a different tidal radius and mass-loss rate compared to circular orbits. However, by extrapolation of the results presented in Webb et al. (2013), when the eccentricity is small ($e \leq 0.25$), as is the case for Fornax with $e = 0.22$, the tidal radius of a stellar system can be approximated by that of a circular orbit with a radius equal to the perigalactic distance of the elliptic orbit. As a result, we approximate the Fornax effective tidal radius by replacing R_G in equation (3) with the perigalactic distance of Fornax orbit ($R_p = 99.4$ kpc). Depending on the model that we have adopted for the density profile of Fornax, we obtain different total masses and different tidal radii which are listed in Table 1. Cuspy models have an average tidal radius of $R_t \approx 3.9$ kpc (comparable with $R_t = 3.6$ kpc from Walcher et al. 2003), whereas the tidal radius of the LC model is $R_t = 6.7$ kpc owing to its larger total mass. For comparison, by fitting King (1966) truncated models to the density profile of Fornax, Irwin & Hatzidimitriou (1995) derived a tidal radius of $71.'1 \pm 4.'0$ for Fornax, which corresponds to a tidal radius of 3.1 ± 0.16 kpc at the current distance of 149.3 kpc (derived in Section 2.1) for Fornax .

2.3 Initial conditions of runaways stars

Our assumption is that runaway stars initially belong to one of the Fornax GCs and become unbound by some unknown mechanism. As a result, they all have the same initial distance from the centre of Fornax. In our simulations, the initial speed of each runaway star corresponds to its excess speed, i.e. its speed when it is infinitely far from the cluster and is no longer effected by its gravitational pull. As a result, we don't consider the gravitational effect of the GCs on these runaway stars. Nor do we consider the gravitational interaction between stars. The runaway stars only feel the gravitational force of Fornax and the Milky Way.

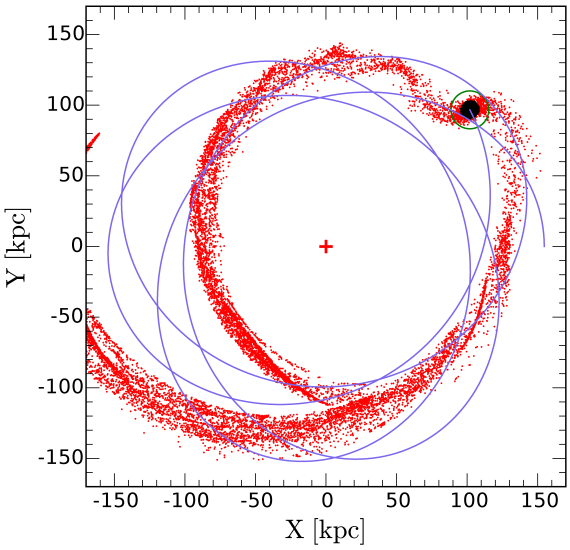

Figure 2. Spatial distribution of stars in the halo of the Milky Way for the LC model after one Hubble time. The Milky Way is denoted by the central cross at the origin. In this simulation, the initial distance of the stars from the centre of Fornax is $R = 3.0$ kpc and their initial speed is $v = 35$ km s^{-1}. Red points represent stars which have left Fornax (about 70 per cent mass-loss). The clump of black points enclosed by the green circle shows stars which still reside within the tidal radius of Fornax. The radius of the green circle is equal to 2 times the tidal radius of Fornax at perigalacticon. The Rosette like orbit of Fornax is shown by the blue solid line. In this figure, X and Y correspond to the coordinate of stars in the orbital plane of Fornax and not the Galactocentric rest frame defined in Section 2.1.

We have $N = 20000$ stars in each simulation and give all of them the same initial speed and the same initial distance from the centre of Fornax. The orientation of the velocity vector of each runaway star is determined from its speed and a uniform spherical distribution. For the whole grid of runs we vary the speed of runaway stars from 0.0 to 50.0 km s^{-1} spaced by 0.5 km s^{-1}. The initial distance of the stars varies from 0.5 to 3.0 kpc for cuspy models and 3.0 to 6.0 kpc for the LC model, spaced by 0.5 kpc. These values are below the tidal radius of Fornax for each density profile. The initial position of Fornax is set to its apogalacticon in each simulation.

We let the simulations run for $T = 13.8$ Gyr and determine the fraction of stars lost from Fornax using the tidal

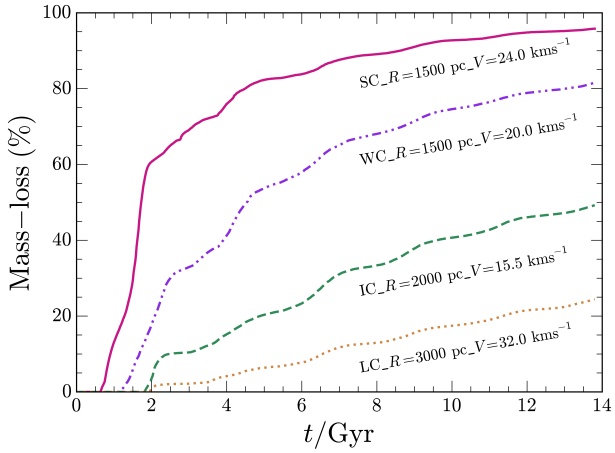

Figure 3. Mass-loss as a function of time for 4 different simulations. The first entry in the label of each simulation is the adopted model for the density profile of Fornax, the second entry is the initial distance of the stars from the centre of Fornax (equal to the orbital radius of GCs) and the last entry is the initial speed of the stars. Note how the LC model has a lower mass-loss compared to other models for $R < 3.0$ kpc. For models with significant mass-loss, the major mass-loss happens in the first 5 Gyr, followed by a slow rise afterwards.

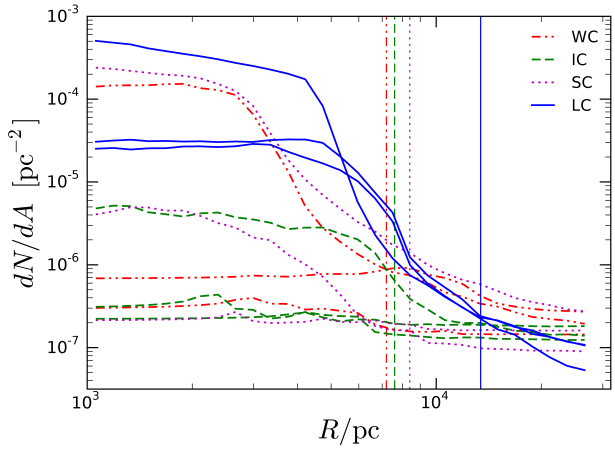

Figure 4. Surface density of stars as a function of projected radius for different models after a Hubble time calculated using infinite projections method (Mashchenko & Sills 2005). The vertical lines mark $2R_t$ where R_t is the tidal radius of Fornax at perigalacticon according to different models. The densities are almost constant inside Fornax and they drop beyond R_t and start to level off beyond $2R_t$ as they reach the background density. Curves with the same color and line style correspond to the same density profile for Fornax but differ in model parameters, i.e. different initial orbital radii and initial speed for stars. The parameters for the models shown in this figure are (from the top to the bottom for each density profile) WC: (2.5 kpc, 15 km s^{-1}), (1.5 kpc, 35 km s^{-1}), (1.0 kpc, 30 km s^{-1}); IC: (2.5 kpc, 20 km s^{-1}), (1.5 kpc, 27 km s^{-1}), (1.0 kpc, 35 km s^{-1}); SC (1.5 kpc, 35 km s^{-1}), (2.5 kpc, 15 km s^{-1}), (1.5 kpc, 25 km s^{-1}); LC: (4.5 kpc, 15 km s^{-1}), (5.5 kpc, 25 km s^{-1}), (3.5 kpc, 35 km s^{-1}).

radii found in Section 2.2. We consider all the stars with $R > 2R_t$ to find the total mass-loss at each snapshot where R_t is the tidal radius of Fornax.

3 RESULTS

Figure 2 shows the distribution of runaway stars with respect to the Milky Way after a Hubble time for one of the LC simulations, with $R_{GC} = 3.0$ kpc and $v = 35$ km s^{-1}. According to this figure, a fraction of stars (~ 30 per cent) will remain in Fornax and the rest leaves Fornax due to their large velocities. The evolution of mass-loss over a Hubble time is depicted in Fig. 3. For the runs with a large mass-loss (> 70 per cent), the majority of runaway stars escape Fornax after only 5 Gyr after which the mass-loss increases only slowly.

Figure 4 shows the projected number density of stars calculated using the infinite projections method of Mashchenko & Sills (2005) which reduces the random fluctuations caused by low number statistics. The densities are almost constant inside Fornax ($R < R_t$) and then rapidly decrease outside the tidal radius. Beyond $R > 2R_t$ the density curves tend to a constant value which is equal to the background density.

The whole grid of our N-body simulations is given in Fig. 5 which illustrates the mass-loss from the Fornax dSph as a function of initial speed and the initial distance of the stars from the centre of Fornax. Mass-loss increases for larger radii and larger speeds, which is the direct consequence of Fornax potential field to become weaker at larger radii. Using this grid, one can estimate the mass-loss which could have happened in Fornax, provided that the initial orbital radii of Fornax GCs are known.

The current projected distances of Fornax GCs from the centre of the dSph are 1.60 kpc, 1.05 kpc, 0.43 kpc, 0.24 kpc and 1.43 kpc (Mackey & Gilmore 2003) and they are all old, with ages ranging from 7 to 14 Gyr (Strader et al. 2003; Mackey & Gilmore 2003). This is puzzling since the GCs are moving in a dark matter halo which can cause dynamical friction and shrink the orbital radius of Fornax GCs within a Hubble time. Yet we don't see any cluster merging in the centre of Fornax and there is no evidence of a bright stellar nucleus in the dSph. This is commonly referred to as the timing problem of Fornax GCs. Cole et al. (2012) studied this problem and generated a wide range of initial conditions for the orbit of Fornax GCs. They showed that, in case of a cuspy density profile for Fornax (i.e. WC, IC and SC models), when the initial orbital radii of Fornax GCs are less than $2-3$ kpc, the orbital radii of Fornax GCs significantly decrease as a result of dynamical friction after only 2 Gyr. In addition, all clusters except for Fornax 1 will fall into the centre of Fornax over a Hubble time. Since Fornax GCs are located at radii far from the central region of the dSph (i.e. $r > 200$ pc), this implies that the initial orbital radii of clusters must have been larger than their current orbital radii, i.e. they all have initial orbital radii of ≥ 2 kpc. Otherwise, they must have fallen into the centre of the dSph and merge by now. This can be seen from figure 4 of Cole et al. (2012) which shows the evolution of the orbital radii of Fornax GCs for different density profiles. In contrast, the infall of the clusters does not happen in case of the LC model.

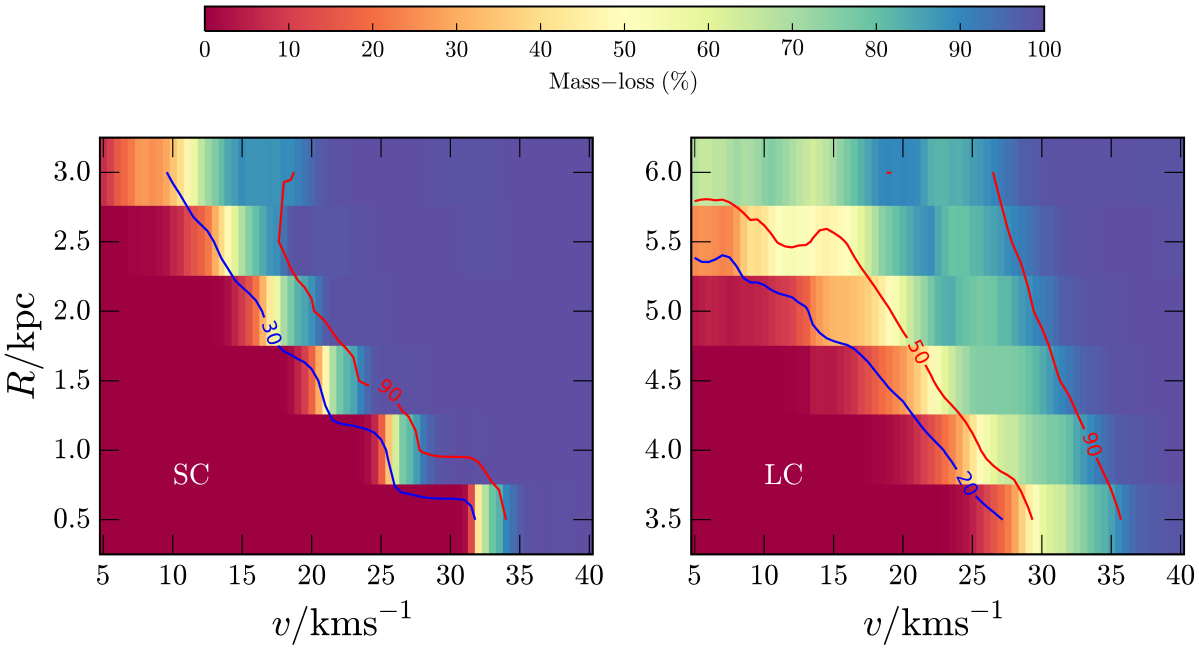

Figure 5. Mass-loss from Fornax as a function of the initial velocity and the initial distance of stars from the centre of Fornax for SC and LC models. WC and IC models have a very similar pattern to the SC model. The LC model predicts a lower mass-loss compared to cuspy models for $R < 3.0$ kpc.

GCs in this model show a dynamical buoyancy instead of dynamical friction as shown by Cole et al. (2012). It can be inferred from figure 4 of Cole et al. (2012) that Fornax GCs formed more or less at the same radii as they are seen today ($R < 1.5$ kpc) in this case.

Knowing that the initial orbital radii of GCs must be either $2-3$ kpc or ~ 1.5 kpc depending on the density profile, what remains is to see at what radius the runaway stars are released. The significant mass-loss of the GCs occurs over a time-scale of the order of Myrs (see Section 4). This is much smaller than the dynamical evolution time-scale of the orbits due to dynamical friction/buoyancy which is of the order of Gyrs (Cole et al. 2012). As a result one can assume that when the significant mass-loss happened in Fornax GCs, the runaway stars were released with an initial orbital radius equal to that of the cluster, i.e. $2-3$ kpc for cuspy models and ~ 1.5 kpc for the LC model.

Combining these facts with Fig. 5, one can see that for all of the cuspy models, mass-loss can be as high as 90 per cent for $R = 2-3$ kpc and $v > 20\,\mathrm{km\,s^{-1}}$, whereas for the large core model this value is less than 10 per cent. This indicates that the LC model systematically predicts a lower mass-loss at the same radii compared to cuspy models (also evident in Fig. 3). To achieve the same mass-loss from Fornax in case of the LC model, the speed of stars need to be $v > 35\,\mathrm{km\,s^{-1}}$ at $R = 2-3$ kpc. The reason that the LC model has a lower mass-loss is due to its larger enclosed mass at each radius which leads to a larger gravitational force compared to cuspy models. This can also be inferred from Fig. 1 which shows that the LC model has a larger circular velocity for $R > 0.8$ kpc.

4 IMPLICATIONS FOR FORMATION SCENARIOS OF CHEMICALLY PECULIAR STARS

So far, two mechanisms have been suggested to produce a significant mass-loss from GCs: stellar evolution induced mass-loss in extended clusters (DE08) and primordial gas expulsion (KB15). In this section, we estimate the mass-loss which can be achieved by both of these mechanisms based on our results given in Section 3.

4.1 Gas expulsion

In this section we test whether we can achieve a high mass-loss from Fornax if runaway stars are a result of gas expulsion in GCs.

In KB15, we did N-body simulations of GCs with two stellar populations to study the role of primordial gas expulsion on the mass-loss. Using a series of Monte Carlo simulations, we then compared the simulated GCs with Galactic clusters and found that gas expulsion induced mass-loss can explain the large fraction of chemically peculiar stars in GCs, as well the observed distribution for the current mass and the half-mass radius of the Galactic GCs. Assuming that all Galactic GCs have undergone gas expulsion induced mass-loss, we found an upper limit of 10^5 yr for the gas expulsion time scale. In addition, we found that the typical initial stellar masses, half-mass radii and the initial mass of the primordial gas left in the Galactic GCs need to be around $10^6\,\mathrm{M}_\odot$, 1.0 pc and $10^6\,\mathrm{M}_\odot$ respectively, so the total mass of each cluster is $\sim 2\times10^6\,\mathrm{M}_\odot$.

To estimate the mass-loss from Fornax as a result of gas expulsion in Fornax GCs, we use the KB15 grid of N-body simulations. Our assumption is that the initial mass

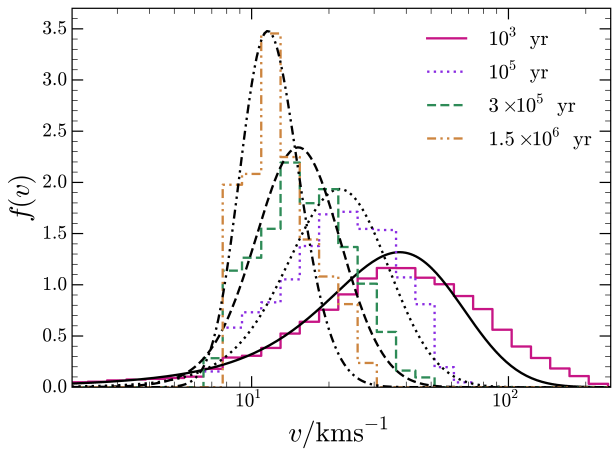

Figure 6. The normalized distribution of excess speeds of runaway stars for an isolated cluster with an initial stellar mass of $M_\star = 10^6\,\mathrm{M}_\odot$ and an initial half-mass radius of $R_\mathrm{h} = 1.0\,\mathrm{pc}$ for different gas expulsion time-scales. Data is taken from KB15. The black lines show the best Gumbel fit to the data whose probability density function is given by $f(v) = \frac{1}{\sigma}\exp\left(-\frac{v-\mu}{\sigma} - \exp\left(-\frac{v-\mu}{\sigma}\right)\right)$, where μ and σ are location (mode) and scale parameters of the distribution.

and half mass radii of Fornax GCs are similar to those of Galactic GCs, i.e. $R_\mathrm{h} = 1.0\,\mathrm{pc}$ and $M_\mathrm{c} = 2\times10^6\,\mathrm{M}_\odot$. We then need the ratio of tidal radii of the GCs to their half-mass radii to completely identify the location of Fornax GCs in the N-body grid of KB15. We calculate the tidal radius of the GCs in the potential field of Fornax using the following equation

$$R_\mathrm{t} = M_\mathrm{c}^{\frac{1}{3}}\left(3\frac{M(R_\mathrm{G})}{R_\mathrm{G}^3} - 4\pi\rho(R_\mathrm{G})\right)^{-\frac{1}{3}} \quad (4)$$

where $M_\mathrm{c} = 2\times10^6\,\mathrm{M}_\odot$ is the total mass of each cluster and $M(R_\mathrm{G})$ is the enclosed mass of Fornax within R_G and needs to be found by numerical integration. The derivation details of this equation are given in Appendix B.

Using equation (4), we found that the tidal radii of our clusters in the tidal field of Fornax are larger than 100 pc for orbital radii $R > 0.5\,\mathrm{kpc}$ for all density profiles of Fornax. Such a large tidal radius corresponds to an almost isolated cluster as can be seen from figures 1 to 3 of KB15. As a result we take the data of isolated clusters from KB15 and find the distribution of excess speeds for runaway stars. Figure 6 shows the normalized distribution of excess speeds for different gas expulsion time-scales. As it can been seen from this figure, lower gas expulsion time-scales lead to faster excess speeds. In addition, for $T_\mathrm{exp} \leq 10^5\,\mathrm{yr}$, they have a mean excess speed larger than $20\,\mathrm{km\,s^{-1}}$, indicating that it is possible to achieve a significant mass-loss with gas expulsion.

To determine the extent of mass-loss as a function of the gas expulsion time-scale and the orbital radii of GCs, we did an analysis as follows: For each runaway star we randomly draw a value from the excess speed distribution assuming a particular gas expulsion time-scale (Fig. 6). We then find the velocity vector of the runaway star using its excess speed and a uniform spherical distribution for its orientation in space. We then add the velocity of the star to the velocity of the GC around Fornax at each radius (circular velocity) and the velocity of Fornax around the Milky Way. Finally, we derive the speed distribution of the runaway stars from their velocity vectors and convolve this distribution with our grid in Fig. 5.

Figure 7 shows the mass-loss as a function of the GCs orbital radii and gas expulsion time-scales. As it can be seen from this figure, depending on the density profile of Fornax, the gas expulsion time-scale and the initial orbital radius of the cluster, mass-loss from Fornax varies from 30 to more than 90 per cent. As a result, with gas expulsion, it is possible that the majority of the runaway stars leave the Fornax galaxy without contributing to the metallicity distribution of field stars. The implication of these results is further discussed in section 5.

4.2 Stellar evolution induced mass-loss

We compare the results obtained in Section 4.1 with the DE08 models for clusters with $M_\mathrm{c} = 10^6\,\mathrm{M}_\odot$ to find the typical excess speed of runaway stars which become unbound as a result of stellar evolution. DE08 used hydrodynamical and N-body simulations, to model the formation and dynamical evolution of multiple stellar populations in GCs, based on the AGB scenario and the stellar evolution induced mass-loss caused by the supernovae ejecta of primordial stars. In their models, GCs have King (1966) density profiles with core, half-mass and tidal radii of $R_\mathrm{c} = 2.85$, $R_\mathrm{h} \sim 10.3\,\mathrm{pc}$ and $R_\mathrm{t} = 90\,\mathrm{pc}$ respectively and they lose a substantial amount of their mass during a period of $10-100$ dynamical times. These models can explain the large fraction of chemically peculiar stars in GCs. However, one needs very extended clusters ($R_\mathrm{h} \sim 10.3\,\mathrm{pc}$) to lose a substantial amount of mass.

To estimate the typical excess speed of runaway stars in DE08 models, we take the typical excess speeds found in Section 4.1 and then scale them to the models of DE08, using the mass and the radius of the clusters. The dynamical time-scale of a cluster and the velocity dispersion of its stars is proportional to $T_\mathrm{dyn} \propto M^{-1/2}R^{3/2}$ and $\sigma_v \propto (M/R)^{1/2}$ respectively. The models that we studied in Section 4.1 have $M_\mathrm{c} = 2\times10^6\,\mathrm{M}_\odot$, $R_\mathrm{h} = 1.0\,\mathrm{pc}$ and $T_\mathrm{dyn} = 3\times10^4\,\mathrm{yr}$. This corresponds to a mass and radius ratio of $M_\mathrm{c}(\mathrm{DE08})/M_\mathrm{c}(\mathrm{KB15}) = (10^6\,\mathrm{M}_\odot)/(2\times10^6\,\mathrm{M}_\odot) = 0.5$ and $R_\mathrm{h}(\mathrm{DE08})/R_\mathrm{h}(\mathrm{KB15}) = (10.3\,\mathrm{pc})/(1.0\,\mathrm{pc}) = 10.3$ respectively. As a result, the velocity dispersion of stars in DE08 models is smaller than that of KB15 by a factor of $(0.5/10.3)^{-1/2} \sim 4.5$, and the dynamical time-scale of the clusters is larger by a factor of $0.5^{-1/2}\times10.3^{3/2} \sim 47$. In case of impulsive mass-loss, these values correspond to a mass-loss time-scale of at least $47\times3\times10^4\,\mathrm{yr} = 1.5\,\mathrm{Myr}$. In Fig. 6, the dash-dotted curve corresponds to a gas expulsion time-scale of $T = 1.5\,\mathrm{Myr}$. According to this curve the typical excess speed of stars is $\sim 12\,\mathrm{km\,s^{-1}}$ for Khalaj & Baumgardt (2015) models. We found that the velocity dispersion of stars in the models of DE08 is smaller by a factor of ~ 4.5, this translates into a typical excess speed of $12/4.5 = 2.6\,\mathrm{km\,s^{-1}}$ for DE08 models. Assuming that the unbound stars have a speed distribution similar to Fig. 6 and applying the same procedure explained in Section 4.1, we obtain a mass-loss of less than ~ 30 per cent from Fornax for $R = 3.0\,\mathrm{kpc}$ and cuspy models. This upper limit on mass-loss which is smaller for clusters with $R < 3.0\,\mathrm{kpc}$, is significantly lower than what we obtained for gas expulsion, indicating that the mecha-

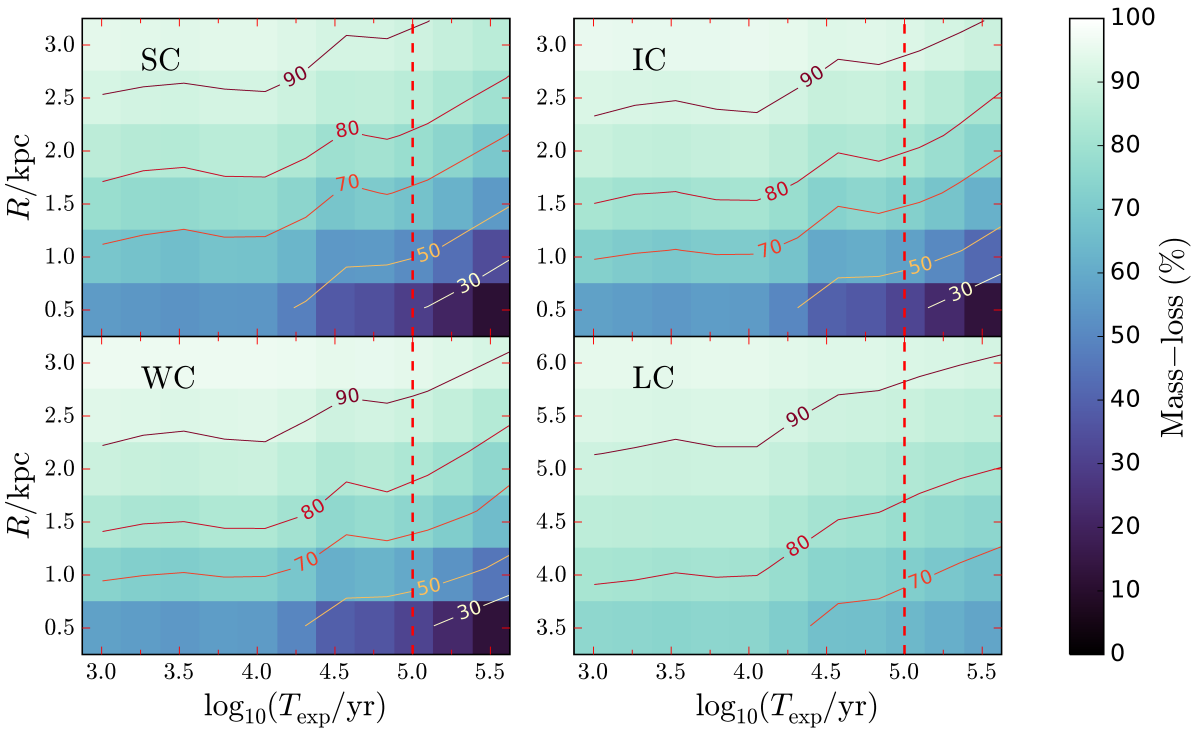

Figure 7. Mass-loss from Fornax as a function of cluster orbital radius and gas expulsion time-scale for different models. The LC model predicts a lower mass-loss compared to cuspy models for $R < 3.0$ kpc. The vertical dashed line marks the upper limit on gas expulsion time-scale found in KB15.

nism proposed by DE08 is not efficient in expelling unbound stars from the Fornax dSph.

5 DISCUSSION AND CONCLUSIONS

Using a series of N-body simulations we determined the mass-loss from the Fornax dSph as a function of the initial speed and the initial distance of stars from the Fornax centre. We assumed a set of cuspy and cored models and tracked the trajectory of stars over a Hubble time. We then combined our results with those of D'Ercole et al. (2008) and Khalaj & Baumgardt (2015) to test whether significant mass-loss could have happened in Fornax GCs. Our results show that gas expulsion induced mass-loss in contrast to stellar evolution induced mass-loss can lead to large excess speeds for runaway stars and larger mass-loss from Fornax.

In particular, in case of gas expulsion induced mass-loss in GCs and for cuspy models when the orbital radii of GCs are between $2-3$ kpc, a mass-loss of ~ 90 per cent can be achieved from Fornax. Comparing this result with the fact that Fornax GCs could have been 4-5 times more massive initially (Larsen et al. 2012), means that Fornax GCs could have lost a significant fraction (> 95 per cent) of their initial mass and still yield a metallicity distribution of field stars which is consistent with observations. This result is especially important for Fornax 3 which is the most massive cluster in Fornax and imposes the tightest limit on the mass-loss from GCs in this galaxy.

In contrast, this is not the case for the LC model. GCs in this model, as shown by Cole et al. (2012) formed at the same radii as they are seen today ($R < 1.5$ kpc) in which case the maximum mass-loss attained for LC model will be less than 50 per cent. A large core with $R_{\rm c} \sim 1.5$ kpc, overestimates the overall mass of the Fornax which is found to be $\sim 1-3\times10^8\,{\rm M}_\odot$ by several studies (e.g. Irwin & Hatzidimitriou 1995; Walcher et al. 2003; Lokas 2009). In addition, Strigari et al. (2006) showed that such a large core for Fornax will be inconsistent with standard warm and dark matter models and predicts an unreasonably massive dark matter halo and a large asymptotic velocity of 200 km s^{-1}. However there are studies which prefer a cored model of $R_{\rm c} \sim 1.0$ kpc (e.g. Amorisco et al. 2013) and it seems that different cored-cuspy models are possible to describe the dark matter profile of Fornax.

We showed that, if Fornax has a cuspy density profile or a small core, then it is possible to reconcile the predictions of significant mass-loss scenario (Khalaj & Baumgardt 2015) with the observed metallicity distribution of field stars in Fornax (Larsen et al. 2012).

We have done our simulations based on the assumption that the potential field of the Milky Way and Fornax are constant in time. This might not be true, especially for Fornax which has been suggested to be the remnant of a recent merging event (Coleman et al. 2004; Yozin & Bekki 2012; del Pino et al. 2015). In such a case, the present-day metallicity distribution of field stars does not directly reflect the mass-loss history of GCs in Fornax and the upper limit for the initial mass of Fornax GCs estimated by Larsen et al. (2012) does not apply.

ACKNOWLEDGEMENTS

We would like to thank the anonymous referee for his/her useful comments and suggestions which improved the quality of this work. PK and HB are members of international team 271 "Massive star clusters across the Hubble time" led by Corinne Charbonnel in the International Space Science Institute (ISSI), Bern, Switzerland. PK and HB would like to appreciate ISSI funding and hospitality during the team meetings in January 2014 and June 2015.

REFERENCES

Amorisco N. C., Agnello A., Evans N. W., 2013, MNRAS, 429, L89
Bastian N., Lardo C., 2015, MNRAS, 453, 357
Bastian N., Lamers H. J. G. L. M., de Mink S. E., Longmore S. N., Goodwin S. P., Gieles M., 2013, MNRAS, 436, 2398
Bastian N., Cabrera-Ziri I., Salaris M., 2015, MNRAS, 449, 3333
Baumgardt H., Makino J., 2003, MNRAS, 340, 227
Bertin G., Varri A. L., 2008, ApJ, 689, 1005
Carretta E., Bragaglia A., Gratton R. G., Recio-Blanco A., Lucatello S., D'Orazi V., Cassisi S., 2010, A&A, 516, A55
Carretta E., et al., 2015, A&A, 578, A116
Cole D. R., Dehnen W., Read J. I., Wilkinson M. I., 2012, MNRAS, 426, 601
Coleman M., Da Costa G. S., Bland-Hawthorn J., Martínez-Delgado D., Freeman K. C., Malin D., 2004, AJ, 127, 832
D'Antona F., Caloi V., D'Ercole A., Tailo M., Vesperini E., Ventura P., Di Criscienzo M., 2013, MNRAS, 434, 1138
D'Ercole A., Vesperini E., D'Antona F., McMillan S. L. W., Recchi S., 2008, MNRAS, 391, 825
Decressin T., Meynet G., Charbonnel C., Prantzos N., Ekström S., 2007a, A&A, 464, 1029
Decressin T., Charbonnel C., Meynet G., 2007b, A&A, 475, 859
Irrgang A., Wilcox B., Tucker E., Schiefelbein L., 2013, A&A, 549, A137
Irwin M., Hatzidimitriou D., 1995, MNRAS, 277, 1354
Khalaj P., Baumgardt H., 2015, MNRAS, 452, 924
King I. R., 1966, AJ, 71, 64
Krause M., Charbonnel C., Decressin T., Meynet G., Prantzos N., 2013, A&A, 552, A121
Kroupa P., 2001, MNRAS, 322, 231
Larsen S. S., Strader J., Brodie J. P., 2012, A&A, 544, L14
Larsen S. S., Brodie J. P., Forbes D. A., Strader J., 2014, A&A, 565, A98
Łokas E. L., 2009, MNRAS, 394, L102
Mackey A. D., Gilmore G. F., 2003, MNRAS, 340, 175
Mashchenko S., Sills A., 2005, ApJ, 619, 243
McMillan P. J., 2011, MNRAS, 414, 2446
Milone A. P., et al., 2015, ApJ, 808, 51
Pawlowski M. S., Kroupa P., 2013, MNRAS, 435, 2116
Piotto G., et al., 2007, ApJ, 661, L53
Prantzos N., Charbonnel C., 2006, A&A, 458, 135
Renaud F., Gieles M., Boily C. M., 2011, MNRAS, 418, 759
Rey S.-C., Lee Y.-W., Ree C. H., Joo J.-M., Sohn Y.-J., Walker A. R., 2004, AJ, 127, 958
Strader J., Brodie J. P., Forbes D. A., Beasley M. A., Huchra J. P., 2003, AJ, 125, 1291
Strigari L. E., Bullock J. S., Kaplinghat M., Kravtsov A. V., Gnedin O. Y., Abazajian K., Klypin A. A., 2006, ApJ, 652, 306
Ventura P., D'Antona F., Mazzitelli I., Gratton R., 2001, ApJ, 550, L65
Walcher C. J., Fried J. W., Burkert A., Klessen R. S., 2003, A&A, 406, 847
Webb J. J., Harris W. E., Sills A., Hurley J. R., 2013, ApJ, 764, 124
Webb J. J., Leigh N., Sills A., Harris W. E., Hurley J. R., 2014, MNRAS, 442, 1569
Yozin C., Bekki K., 2012, ApJ, 756, L18
de Boer T. J. L., Fraser M., 2015, preprint, (arXiv:1510.05642)
de Mink S. E., Pols O. R., Langer N., Izzard R. G., 2009, A&A, 507, L1
del Pino A., Aparicio A., Hidalgo S. L., 2015, MNRAS, 454, 3996

APPENDIX A: TIDAL RADIUS OF FORNAX

Following the approach and the notation of Renaud et al. (2011), the tidal radius [1] of a stellar system with mass M, on a circular orbit with radius $R_{\rm G}$ around a host galaxy with an arbitrary potential field $\phi_{\rm G}$, can be written as follows (equations 10 and 17 therein)

$$R_{\rm t} = \left(\frac{GM}{\lambda_{e,1}}\right)^{\frac{1}{3}} \tag{A1}$$

where $\lambda_{e,1}$ is the largest eigenvalue of the effective tidal tensor[2] and is given by

$$\lambda_{e,1} = \left(-\frac{\partial^2\phi_{\rm G}}{\partial x^2}\right)_{R_{\rm G}} - \left(-\frac{\partial^2\phi_{\rm G}}{\partial z^2}\right)_{R_{\rm G}} \tag{A2}$$

In the derivation of this equation, it has been assumed that the potential of the stellar system is simply $-GM_{\rm c}/r$ which is a reasonable assumption at the tidal radius (Renaud et al. 2011).

The substitution of the equation (1) into equation (A2) yields

$$\lambda_{e,1} = \frac{2R_{\rm G}^2 V_\infty^2}{\left(R_{\rm c}^2 + R_{\rm G}^2\right)^2} \tag{A3}$$

hence the tidal radius is

$$R_{\rm t} = \left(\frac{GM}{2V_\infty^2}\right)^{\frac{1}{3}} R_{\rm G}^{\frac{2}{3}} \left(\left(\frac{R_{\rm c}}{R_{\rm G}}\right)^2 + 1\right)^{\frac{2}{3}} \tag{A4}$$

One can also use equation 10 of Bertin & Varri (2008) and derive the same formula for the tidal radius.

For $R_{\rm G} \gg R_{\rm c}$, the last term on the right-hand side of the equation (A4) goes to zero and one can approximate the above equation for the logarithmic potential by the following form which is essentially the tidal radius of a system in an isothermal sphere[3] (Baumgardt & Makino 2003)

$$R_{\rm t} \approx \left(\frac{GM}{2V_\infty^2}\right)^{\frac{1}{3}} R_{\rm G}^{\frac{2}{3}}, \quad \frac{R_{\rm G}}{R_{\rm c}} \gg 1 \tag{A5}$$

APPENDIX B: SIMPLIFYING TIDAL RADII EQUATIONS FOR NUMERICAL CALCULATIONS

It is straightforward to calculate tidal radii using equations (A1) and (A2) given an analytical relation for potential. However, when only the matter distribution $\rho(r)$ of the

[1] The distance of the first Lagrangian point (L_1) from the center of the system.
[2] The sum of the tidal and centrifugal potentials.
[3] $\rho(r) \propto r^{-2}$

host galaxy is given in analytical form, one needs numerical integration followed by a numerical second order differentiation to find tidal radii which can be a cumbersome and error-prone process.

To overcome this issue, we have taken advantage of Poisson's equation, assuming spherical symmetry for the density

$$\nabla\phi(r) = 4\pi G\rho(r) \rightarrow \frac{1}{r^2}\frac{d}{dr}\left(r^2\frac{d\phi(r)}{dr}\right) = 4\pi G\rho(r) \tag{B1}$$

Expanding this equation yields

$$\frac{d^2\phi(r)}{dr^2} + \frac{2}{r}\frac{d\phi(r)}{dr} = 4\pi G\rho(r) \tag{B2}$$

where $d\phi(r)/dr$ is simply the magnitude of acceleration at radius r and can be written in terms of the enclosed mass $M(r)$

$$\frac{d\phi(r)}{dr} = G\frac{M(r)}{r^2} \tag{B3}$$

The first derivative of potential with respect to x_i is

$$\frac{\partial\phi(r)}{\partial x_i} = \frac{d\phi(r)}{dr}\frac{\partial r}{\partial x_i} \tag{B4}$$

knowing that $\partial r/\partial x_i = x_i/r$, then the second derivative of ϕ will be

$$\frac{\partial^2\phi(r)}{\partial x_i^2} = \frac{d^2\phi(r)}{dr^2}\left(\frac{x_i}{r}\right)^2 + \left(\frac{1}{r} - \frac{x_i^2}{r^3}\right)\frac{d\phi(r)}{dr} \tag{B5}$$

Substituting equation (B5) into equation (A2) yields

$$\lambda_{e,1} = \frac{1}{r}\frac{d\phi(r)}{dr} - \frac{d^2\phi(r)}{dr^2} \tag{B6}$$

which can be simplified by replacing first and second derivatives of potential with respect to r using equations (B2) and (B3)

$$\lambda_{e,1} = 3G\frac{M(r)}{r^3} - 4\pi G\rho(r) \tag{B7}$$

Hence the tidal radius of a stellar system with mass $M_{\rm c}$, located at distance $R_{\rm G}$ from the centre of the host galaxy will be

$$R_{\rm t} = M_{\rm c}^{\frac{1}{3}}\left(3\frac{M(R_{\rm G})}{R_{\rm G}^3} - 4\pi\rho(R_{\rm G})\right)^{-\frac{1}{3}} = M_{\rm c}^{\frac{1}{3}}\left(3\frac{\Omega(R_{\rm G})^2}{G} - 4\pi\rho(R_{\rm G})\right)^{-\frac{1}{3}} \tag{B8}$$

where $\Omega(R_{\rm G})$ is the orbital angular velocity at $R_{\rm G}$

$$\Omega(R_{\rm G}) = \sqrt{G\frac{M(R_{\rm G})}{R_{\rm G}^3}}$$

Note that, when $\rho(r)$ is known, equation (B8) only needs one integration, for the enclosed mass of the host galaxy within $R_{\rm G}$, to calculate the tidal radius.

This paper has been typeset from a TEX/LATEX file prepared by the author.